Versatile Tetrablock Copolymer Scaffold for Hierarchical Colloidal Nanoparticle Assemblies: Synthesis, Characterization, and Molecular Dynamics Simulation

Gema Marcelo, Fraser Burns, Tânia Ribeiro, J. M. G. Martinho, M. Pilar Tarazona, Matthew G. Moffitt, … & José Paulo S. Farinha

July 2017

A Versatile Tetrablock Copolymer Scaffold for Hierarchical Colloidal Nanoparticle Assemblies: Synthesis, Characterization, and Molecular Dynamics Simulations

Gema Marcelo[a #], Fraser Burns[b #], Tânia Ribeiro[a], J. M. G. Martinho[a], M. Pilar Tarazona[c], Enrique Saiz[c*], Matthew G. Moffitt[b*] and José Paulo S. Farinha[a*]

[a] Centro de Química-Física Molecular and IN-Institute for Nanoscience and Nanotechnology, Instituto Superior Técnico, University of Lisbon, 1049-001 Lisboa, Portugal. [b] Department of Chemistry, University of Victoria, P.O. Box 1700, Stn CSC, Victoria, BC, Canada V8W 3V6. [c] Departamento de Química Física, Universidad de Alcalá, 28871 Alcalá de Henares, Madrid, Spain

* Corresponding authors. E-mail: farinha@tecnico.ulisboa.pt; mmoffitt@uvic.ca; enrique.saiz@uah.es

[#] Gema Marcelo and Fraser Burns contributed equally to this work

Keywords: block copolymers, polyelectrolytes, self-assembly, polymer micelles, cadmium selenide, quantum dots, thiol-functionalized, reversible addition fragmentation chain transfer (RAFT), size-exclusion chromatography-multi-angle light scattering (SEC-MALS), molecular dynamics.

Abstract

A unique combination of molecular dynamics simulations and detailed multi-angle light scattering size exclusion chromatography (SEC-MALS) analysis is used to provide important *a priori* insights into the solution self-assembly of a well-defined and symmetric tetrablock copolymer with two acrylic acid outer blocks, two polystyrene inner blocks and a trithiocarbonate (TTC) central group, prepared by reversible addition-fragmentation chain transfer (RAFT) polymerization. SEC-MALS experiments show that the copolymer forms aggregates in both tetrahydrofuran (THF) and *N*-dimethylformamide (DMF), even in the presence of different salts, but not in 1,4-dioxane (dioxane). Combined with molecular dynamic simulations, these results indicate that the acrylic acid units are the main cause of aggregation through intermolecular hydrogen bonding, with additional stabilization by the central TTC. The block copolymer chains self-assemble in dioxane by adding cadmium acetate, originating flower-like inverse micelles with a cadmium acrylate core and the TTC groups in the outer surface of the PS corona. The micelles were used as nanoreactors in the templated synthesis of a single cadmium selenide quantum dot in the core of each micelle, while the shell TTC groups can be converted into thiol functions for further use of these units in hierarchical nanostructures. Only in dioxane where simulations and SEC-MALS suggest an absence of copolymer aggregates prior to cadmium acetate addition do well-dispersed and highly luminescent CdSe QDs form by templated synthesis. These results provide valuable insights into the self-assembly of RAFT copolymers in different solvent systems as it relates to the preparation of emissive QDs with polymer-spaced thiol functionality for binding to gold nanostructures.

Introduction

Block copolymers of precise architecture and chain length self-assemble into micelles of low size dispersity, which can be used as templates for the growth of metal or semiconductor nanostructures.[1-7] The resulting nanostructures can be used as building blocks in the preparation of hierarchical hybrid nanostructures through subsequent self-assembly mechanisms mediated by the surrounding polymer brushes.[8-12] In particular, nanostructures consisting of a quantum dot (QD) core surrounded by a polymer brush layer terminated with thiol groups are potential building blocks for controlled assemblies of photoluminescent QDs and gold nanostructures with controlled distances mediated by the polymer chains.[12~~12~~] Such composite nanostructures exhibiting controlled interactions between QD emission and gold nanoparticle surface plasmons offer numerous applications as functional elements for sensing and photonics.[8~~8~~,12~~12~~-23]

Formatted: Endnote Reference

Formatted: Endnote Reference

Formatted: Endnote Reference

To achieve fine control over nanoparticle size and spacing in hierarchical hybrid nanostructures, block copolymers with well-defined architectures, predetermined molecular weights, narrow molecular weight distributions, and predictable micellization behaviors in selective solvents, are required. Controlled radical polymerization (CRP) techniques [24,25] have become increasingly popular for the production of polymers with these properties, from a much larger variety of monomers and under simpler polymerization conditions than other controlled polymerization techniques, such as anionic polymerization. All the main CRP techniques, NMP (nitroxide mediated polymerization),[26] ATRP (atom transfer radical polymerization),[27, 28] and RAFT (reversible addition-fragmentation chain transfer),[29-32] can be used to prepare amphiphilic copolymers. These have attracted much attention because of their versatile self-assembly behavior, which can be controlled by different factors, such as the absolute and relative block lengths, the presence of additives, temperature, and the nature and composition of the solvent.[33] Asymmetric poly(styrene-*b*-acrylic acid) copolymers with different

compositions have been used to prepare several supramolecular structures, such as rods, micelles, tubules, onions, spindles and vesicles.[34-38]

Our group has previously applied symmetric amphiphilic tetrablock copolymers of poly(acrylic acid-*b*-styrene-*b*-styrene-*b*-acrylic acid), with a central group of trithiocarbonate (TTC) between the two styrene blocks (PAA-PS-TTC-PS-PAA, Scheme 1) to prepare hierarchical quantum dot (QD)-gold nanoparticle assemblies with surface plasmon-enhanced fluorescence.[12~~12~~] The tetrablock copolymers with central TTC groups were shown to be suitable building blocks for the self-assembly of complex supramolecular assemblies with ensemble properties governed by structural hierarchy. In that work, we induced self-assembly of the copolymer in Scheme 1 into flower-like reverse micelles by adding cadmium acetate. These structures, with a cadmium acrylate core and a polystyrene (PS) shell decorated with the TTC groups, were then used in the templated conversion of the entrapped Cd^{2+} ions to a single CdS QD in each micelle core. The TTC were converted to thiol groups and used to bind gold nanoparticles, leading to polymer-mediated spacing between nanoparticles and gold-enhanced photoluminescence (PL) of the CdS QDs.

Formatted: Endnote Reference

In this paper, we show that a combination of synthesis by sequential RAFT polymerization, characterization by size exclusion chromatography-multi-angle laser light scattering detection (SEC-MALS) and modeling by molecular dynamics (MD) simulations, allows symmetric PAA-PS-TTC-PS-PAA copolymers to be prepared with both precise control and detailed understanding of the various interactions involving the copolymer blocks and the surrounding medium. These features are critical to establishing a versatile polymeric template on which to prepare a myriad of nanoparticle assemblies with finely-tuned distant-dependent interactions. In an effort to develop generalized approaches for templated functional nanostructures, we extend our previous demonstration of templated CdS QD synthesis [12] to the preparation of cadmium selenide (CdSe) QDs surrounded by solvated PS chains terminated by thiol functional groups. Compared to CdS QDs, CdSe QDs are much more common QD

emitters in biophysical and photonic applications, due to their broader range of color tuneability in the visible spectral region.[39-41] We find significant solvent dependencies in the size, colloidal stability, and photoluminescence of the QD-containing RAFT block copolymer colloids, which lead us to a detailed study combining SEC-MALS experiments and MD simulations on analogous oligomers. The results provide valuable insights into the self-assembly of RAFT copolymers in different solvent systems as it relates to the preparation of emissive QDs with polymer-spaced thiol functionality. Thus, the combination of synthetic control, thermodynamic/structural understanding, and chemical versatility presented here, provides a powerful framework for color-tuned PL emission of QDs[39] with enhancements governed by polymer-mediated distances from chemically-bonded gold nanostructures. The CdSe QD micelles described herein and RAFT-based copolymers in general represent promising building blocks for future applications in functional optoelectronic devices, imaging probes, biomarkers, and sensors.

Formatted: Endnote Reference

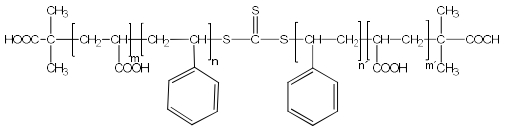

Scheme 1. Block copolymer PAA-*b*-PS-TTC-PS-*b*-PAA obtained by RAFT polymerization.

Experimental

Materials for Polymer Synthesis. Carbon disulphide, chloroform, and acetone from Riedel-de-Haen, tetrabutylammonium hydrogen sulphate and diethyl ether from Fluka, *N*,*N*-dimethylformamide (DMF, PA) and tetrahydrofuran (THF, 99%) from Sigma-Aldrich, trioxane (99%) and 4,4'-azobis(4-cyanovaleric acid) (ACVA, >98%) from Acros, and other chemicals obtained from several sources were used without further purification. Acrylic acid and styrene (Sigma-Aldrich) were distilled under vacuum before use.

Materials for SEC-MALS Characterization. THF (99.9 %,), DMF (99.9 %), dioxane (99.9 %), LiBr and LiCl (reagent plus grade), and (trimethylsilyl)-diazomethane were purchased from Sigma-Aldrich.

Materials for Quantum Dot Micelle Synthesis. Dioxane (99.9%), methanol (99.9%) and cadmium acetate dihydrate ($CdAc_2$, 98%) from Sigma-Aldrich and sodium selenide (Na_2Se, 99.8%) from Alfa Aesar, were used without further purification. Deionized water from a Millipore system Milli-Q ≥18 MΩcm was used for the preparation of solutions.

Synthesis of the Poly(acrylic acid)-*block*-polystyrene-TTC-polystyrene-*block*-poly(acrylic acid) Block Copolymer (PAA-*b*-PS-TTC-PS-*b*-PAA). The 4-block copolymer was prepared as previously described. [12~~12~~] We first prepared the RAFT chain transfer agent *S,S'*-bis(α,α'-dimethyl-α''-acetic acid) trithiocarbonate (TTC) following the procedure reported by Lai *et al.* [42] PAA and TTC were used in the RAFT polymerization of a symmetric copolymer with two poly(acrylic acid) blocks (PAA-TTC-PAA, Scheme 2), with number averaged molecular weight M_n = 3000 g mol^{-1} (M_w/M_n = 1.02), corresponding to a degree of polymerization $\langle 2\ n \rangle = 37$.

Formatted: Endnote Reference

The PAA-TTC-PAA copolymer was used as macro-CTA to prepare a PAA-*b*-PS-TTC-PS-*b*-PAA tetra-block copolymer. The RAFT polymerization of styrene resulted in a degree of polymerization $\langle 2\ m \rangle = 115$ (Scheme 1), corresponding to a total copolymer molecular weight of M_n= 14900 g/mol. This was calculated from the 46% monomer conversion obtained by NMR of the polymerization mixture diluted 1:5 in acetone-d6, by comparing the ratios of the integrated peaks of the vinyl protons of styrene and the methyl protons of DMF (used as an internal reference) before and after the polymerization.

Some of the tetra-block copolymer was silylated by adding 2.0 M (trimethylsilyl)-diazomethane in hexane solution, dropwise, into a solution of the PAA-*b*-PS-TTC-PS-*b*-PAA copolymer in THF (100 mg/13 mL THF) at room temperature. [43] Addition of the silylation agent was continued until the

solution became yellow, after which an excess of methylation agent was further added. The reaction mixture was stirred at room temperature for 3 h more before the recovered polymer was injected in the SEC (without purification). To prove the symmetry of the copolymer (see below), we performed the aminolysis of 100 mg of the copolymer by dissolving the sample in 13 mL of THF and adding a 50-fold excess of hexylamine. The reaction was left shaking overnight at room temperature.

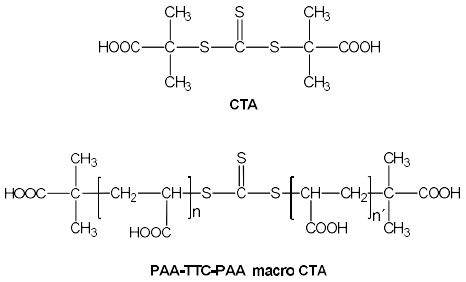

Scheme 2. *S,S'*-bis(α,α'-dimethyl-α''-acetic acid) trithiocarbonate chain transfer agent (CTA) and PAA-TTC-PAA macroCTA.

Preparation and Characterization of Cadmium Selenide Quantum Dot Micelles (QDMs). A sample of the PAA-*b*-PS-TTC-PS-*b*-PAA copolymer was diluted to 0.5 wt% with 1,4-dioxane (dioxane) and allowed to stir overnight at 25ºC in the dark to homogenize. A 0.25 M methanolic cadmium acetate dehydrate solution was added to the polymeric solution in a 1:1 molar ratio of Cd^{2+} to COOH groups (from the PAA), and allowed to stir overnight at 25ºC in the dark. An aliquot (0.5 mL) of this sample was removed and diluted with 4 mL of a 1:1 mixture of toluene to dioxane (v/v) and stirred for 5 hours to homogenize. A 0.052 M solution of sodium selenide (Na_2Se) was prepared through the dilution of 0.013 g of Na_2Se with 2 mL of a 1:1 deionized water to methanol solution. The Na_2Se solution was added to the polymer solution such that the final mixture contained 0.3 moles of Se^{2-} per COOH group (160 μL). This solution was allowed to stir overnight in the dark.

Size Exclusion Chromatography (SEC). SEC measurements were carried out using a Waters Associates equipment with a 510 pump, a 7725 Rheodyne injector and a differential refractive index detector (model 410). The multi-angle light scattering detector (MALS) was a miniDAWN TREOS laser photometer from Wyatt Technology Corp. The working temperature was 30 ºC. Three columns with a non-polar stationary phase (styrene-divinyl benzene copolymers) were generally used: one Styragel HR5 column (5 µm, 7.8 x 300 mm from Waters) and two linear Phenogel columns (5 µm, 7.8 × 300 mm from Phenomenex).[44] For the characterization of the copolymer in DMF and Dioxane and the methylated copolymer in THF only the two linear phenogel columns were used. The flow rate was 1 ml/min for THF, and 0.3 ml/min for DMF and Dioxane and the injector loop was 100 µl.

The refractive index (RI) detector measures the concentration of the polymer and the MALS detector (calibrated with spectrometric grade toluene) measures the excess Rayleigh ratio at different angles for each elution volume fraction of the chromatogram, allowing the calculation of the absolute molecular weight of the polymers. The normalization of the detectors in the different organic solutions was performed with low molecular weight poly(styrene) standards. The shape of the chromatograms obtained with the MALS and the RI detectors are not coincident because the light scattering signal is proportional to the product of the polymer molecular weight and concentration, while the RI signal is proportional to the polymer concentration only.

To make sure there is no effect of the concentration on the SEC separation, for each solvent different concentrations were injected, decreasing from 8 mg/ml. In Figure S1 (Supporting Information) we show that the juxtaposed traces of two injections at different concentration of the copolymer in dioxane have almost perfect matches of the MALS signal and the molecular weight calculated for each elution volume, with the refractive index signal reflecting the concentrations of the injected solutions.

SEC-MALS was used to study the aggregation behavior of the copolymer in different solvents: Dioxane; THF; THF with 0.1 M LiBr; THF with 0.2 M LiCl; DMF; and DMF with 0.15 M LiBr. To evaluate the influence of acrylic acid, the polymer was methylated and further analyzed in THF. The values used for the differential refractive index increment d*n*/d*c* at 632.8 nm were those of polystyrene (the major constituent of the polymer), 0.19 in THF, [44][44] 0.165 in DMF, [45] and 0.166 in dioxane. [46]

Formatted: Endnote Reference

Photophysical Characterization. Absorbance and reflectance measurements were performed on a Perkin Elmer Lambda 1050 UV/Vis/NIR spectrophotometer with a wideband 3 detector module. Fluorescence spectroscopy was performed on an Edinburgh Instruments FLS920 spectrometer with a 450W xenon arc lamp and a Hamatsu R5509 photomultiplier tube (PMT) detector. Slit widths were adjusted to achieve a 5 nm resolution, with a dwell time of 0.5 s.

Light Scattering. The static and dynamic light-scattering measurements were conducted on a Brookhaven Instruments Co. BI-200SM research goniometer, with a Brookhaven Instruments Co. Mini-L30 30 mW red (636 nm) compact diode laser. The measurements were carried out in glass cylindrical cells in order to simplify the corrections needed for refractive index variations. The circular vat cell contains decalin to minimize light refraction. The dynamic light scattering (DLS) measurements were analyzed using the analysis package CONTIN (Brookhaven) to determine the translational diffusion coefficient, from which the hydrodynamic diameter (D_h) of the copolymer is calculated.[47] To effectively remove dust from the solvent, this was filtered with Millipore 0.22 μm pore size filters.

Transmission Electron Microscopy (TEM). Transmission electron micrographs were obtained on a JEOL JEM-1400 transmission electron microscope with a LaB_6 filament, equipped with a GatanOrius SC100 camera, with an accelerator voltage of 80 kV. TEM grids were prepared first by cooling an aluminum (Al) block in liquid nitrogen, a 300-mesh carbon-coated Cu TEM grid was placed on the Al block and 10 μL of CdSe QDM solution was dropped onto the grid and quickly immersed in

liquid ethane. Solution was then placed under vacuum until dry. This likely resulted not in sublimation, due to insufficient vacuum, rather evaporation probably occurred.

Molecular Dynamics Computational Methods. The Amber molecular modeling package,[48] including the Amber force field, was employed for all the Molecular Dynamics (MD) simulations. Coulombic potentials were computed by the Ewald sum procedure. [48] Partial charges were assigned to every atom by means of the MOPAC package and the AM1 procedure. [49] A time step δ = 1 fs was employed for the integration algorithm. The MD simulations were performed on Periodic Boundary Conditions (PBC) under NVT conditions (i.e. Canonical Ensemble), with the temperature being kept constant by means of the Berensen [50] thermostat with a coupling factor of 1000 fs. Several exploratory calculations were performed at different temperatures ranging from 300 to 500 K. Finally, it was decided to perform all the calculations at 500 K in order to increase the atomic velocities, thus facilitating the passage over energetic barriers and consequently improving the statistical sampling of all the configurational space. Thus, the system is supposed to be in a hypothetical state in which the atomic velocities correspond to a rather high temperature while the density, interatomic distances, and in general all the equilibrium properties that are governed by the NVT conditions, are those of a much lower temperature. Even if this situation does not correspond to a real state of the system, the results of equilibrium properties obtained by this kind of simulations are much better than those obtained at the lower temperature at which the system will remain in the same energy well practically during the whole simulation. As it is evident, this approximation fails when applied to compute time dependent properties, but this kind of properties are not the goal of the present work.

Scheme 3 shows the structure of the model oligomers used in the MD simulations. The oligomers of type S (SA and SE) are formed by a central trithiocarbonate (TTC) unit, -S-(CS)-S-, flanked on each side by a block of 10 repeat units of styrene followed by a block of 11 repeat units of either acrylic acid (R = H, SA oligomer) or methyl acrylate ester (R = CH_3, SE oligomer). The

oligomers of type C does not contain the central TTC unit, being formed by a central block of 22 units of styrene, flanked by on each side by 11 units of either acrylic acid (R=H, CA oligomer) or methyl acrylate ester ($R = CH_3$, CE oligomer). Meso and racemic configurations of consecutive units were randomly assigned to each chain producing an overall fraction of meso diads $w_m \approx 0.4$. Ten oligomer chains were packed into a cubic box with Periodic Boundary Conditions (PBC), together with 2,000 molecules of the appropriate solvent and, in some cases, 200 molecules of salt (LiCl), to approach the experimental conditions (Table S1, *Supporting Information*).

The length of the PBC box (L) shown in the last column of Table S1 (*Supporting Information*), was adjusted as to reproduce a macroscopic density of *ca.* 0.9 g cm^{-3}, similar to that of the organic solvents. However, each system was initially built within a box having approximately twice the final side length. The size of these initial boxes was progressively decreased, in 0.1 nm steps, by a combination of MD and energy minimization steps performed as follows: after each decrease of the box length, a 60 ps MD simulation was performed, during which the system was slowly warmed up from 0 to 500 K, equilibrated at this temperature during approximately 20 ps, then slowly cooled down to 0 K. Then, the energy of the system was minimized with respect to all internal coordinates with a combination of steepest descendent all conjugated gradient algorithms.[48,48] Once the system has reached the desired volume, it was slowly warmed up during 100 ps from 0 K to 500 K. Finally, the production stage was started for 3×10^6 integration cycles (*i.e.* a time span of 3000 ps), during which the coordinates of the system were recorded at intervals of 1 ps, thus producing a total of 3000 configurations that were further employed in the analysis. The warming step was not considered in the analysis.

Formatted: Endnote Reference

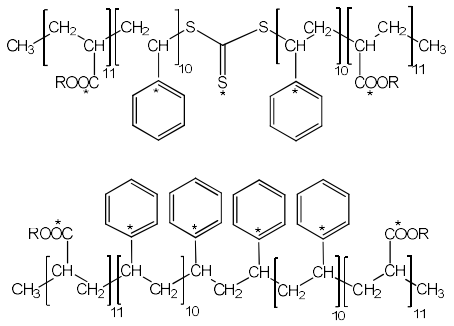

Scheme 3. Schematic representation of oligomer frameworks S (central TTC group, *top*) and C (no central TTC group, *bottom*) used for MD simulations. Based on these two frameworks, four different oligomers were investigated: SA and CA contain acrylic acid repeat units (*i.e.* R = H), while oligomers SE and CE contain methyl acrylate repeat units (*i.e.* R = CH_3).

Results and Discussion

Preparation and Characterization of Cadmium Selenide Quantum Dot Micelles. Three different solvents were tested for the controlled self-assembly of the PAA-*b*-PS-TTC-PS-*b*-PAA copolymer: THF, DMF and 1,4-dioxane. Addition of cadmium acetate to the copolymer in each of the solvents was expected to lead to the formation of inverted micelles with a poly(cadmium acrylate) core and a corona of hydrophobic PS blocks. The hydrodynamic diameter D_h of the micelles prepared by addition of cadmium acetate was measured by dynamic light scattering and analyzed by CONTIN. The intensity distribution of D_h values (which highlight the larger species in dispersion), presented in Figure 1 A-C, show that the intensity-averaged effective hydrodynamic diameters are larger in THF (D_h = 55 nm) than in dioxane (D_h = 39 nm), indicating that, although well-defined micelles are formed in both solvents, these are probably more agglomerated in THF (Figure 1, A and C). For the sample prepared in DMF (Figure 1 B) the intensity-averaged distribution reflects the possible presence of isolated chains and a broad distribution of aggregates.

The presence of isolated chains in the dispersions can be better observed in the number distributions of D_h. The breadth of these distributions (Figure S1) indicate that in the sample prepared in DMF, most of the species in dispersion correspond in fact to unassociated copolymer chains (D_h < 5 nm) and small aggregates with a broad size distribution (*RSD* = 200%). On the other hand, the predominant species in unfiltered samples prepared in dioxane and in THF are block copolymer micellar aggregates of similar and homogeneous size, with the relative standard deviations (*RSD*) of the number distributions showing that the sample prepared in dioxane (*RSD* = 50%) is slightly less heterogeneous than the one in THF (*RSD* = 60%).

We thus conclude that micelles prepared in dioxane are both homogeneous in size (unlike in DMF) and colloidally stable (unlike in THF).

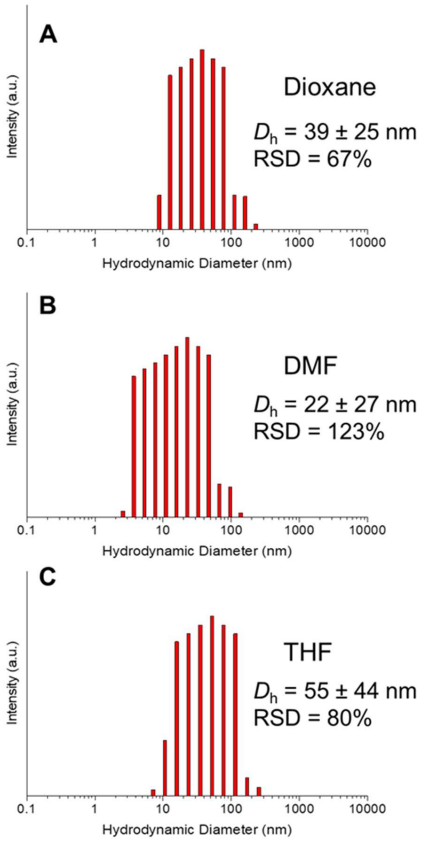

Figure 1. Hydrodynamic diameter intensity distributions obtained by CONTIN analysis of the DLS measurements of cadmium acrylate-core micelles in 1,4-dioxane (A), DMF (B) and THF (C). The average values of D_h were calculated directly from the histograms (presented with the width of the distribution and the corresponding relative standard deviations, *RSD*).

To better understand the relative thermodynamic stability of the cadmium acrylate micelles formed in THF and dioxane, we performed static light scattering (SLS) measurements in tandem with the DLS measurements. The samples were filtered with 0.45 μm Teflon filters to remove any larger aggregates (SLS is especially sensitive to dust and other large scatterers). It was observed that under

identical conditions, only the sample in dioxane was capable of generating a stable dispersion of micelles (Figure S2). In both DMF and THF samples it was not possible to obtain meaningful Zimm plots, probably due to aggregates evolving over time, during the measurements: the small aggregates and the micelle agglomerates previously detected by DLS for DMF and THF samples, respectively.

The SLS measurements of the cadmium acrylate reverse micelles in dioxane indicate a micellar molecular weight M_w = (1.4 ± 1) × 10^6 g·mol^{-1}, a radius of gyration R_g = (24 ± 4) nm and a second-virial coefficient A_2 = (3.4 ± 1.7) ×10^{-5} cm^3·mol·g^{-2}. Although these data were obtained for samples filtered with 0.45 μm Teflon membranes while the intensity-averaged DLS measurements in Figure 1 were performed with unfiltered samples, there is a good correspondence between the these results, with the ratio R_g / (D_h / 2) = 1.2 ± 0.1 indicating a star-like micelle structure with a corona of random coil chains. The second virial coefficient value is small but positive, indicating that the intermicellar interaction is repulsive (i.e. the micelles are stable in dioxane). The meaning of this value can be better understood by expressing the second virial coefficient as a hard-sphere virial diameter, D_{A2}, which corresponds to a sphere where only the excluded volume effect has been taken into account: [47][47]

Formatted: Endnote Reference

$$D_{A2} = 2\left(\frac{3M_W^2 A_2}{16\,\pi\, N_A}\right)^{\frac{1}{3}} \quad (1)$$

where M_w is the molecular weight of the micelles and N_A the Avogadro number. While for noninteracting spherical particles, D_{A2} should be very close to the hydrodynamic dimeter, our micelles in dioxane have D_{A2} = 37.5 nm, [47][47] a value smaller than the intensity-averaged D_h = 39 nm obtained by DLS (Figure 1), as expected for star-like block copolymer micelles with a "soft" outer shell leading to steric stabilization.

Formatted: Endnote Reference

The poly(cadmium acrylate) core of the micelles were then used as nanoreactors to prepare CdSe QDs by adding Na_2Se in an approximately 50/50 (v/v) mixture with toluene. Formation of a CdSe QD at the micelle core originates a quantum dot micelle (QDM, cartoon in Scheme 4) where the

QD is encapsulated by a PS shell. These experiments produced clear yellow colloidal dispersions when 1,4-dioxane was used in the preparation of the micelles (Figure 2A, top). With both DMF and THF we obtained slightly turbid dispersions (Figure 2, B and C, top), which precipitated overnight (Figure S3). Furthermore, the typical emission of CdSe quantum dots (observed under 365 nm illumination in Figure 2, bottom) was only clearly observed for the sample prepared with 1,4-dioxane.

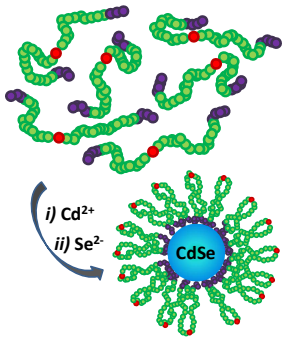

Scheme 4. Cartoon representation of the CdSe quantum-dot micelle (QDM) structure. The PAA-*b*-PS-TTC-PS-*b*-PAA block copolymers self-assemble in dioxane upon addition of $CdAc_2$, forming micelle nanoreactors with a core of cadmium-crosslinked PAA blocks (*purple*) and a flower-like corona of PS blocks (*green*) with a TTC group (*red*) at each "petal". The CdSe QD is formed at the micelle core by addition of Na_2Se.

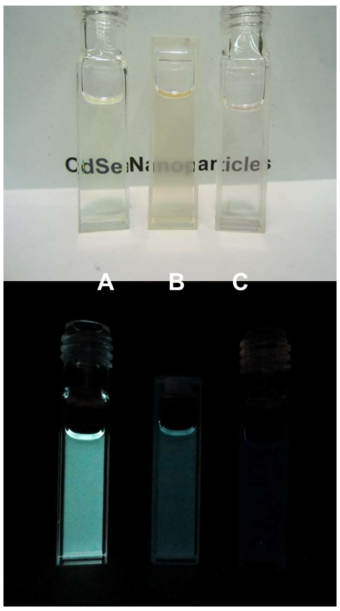

Figure 2. Photographs of CdSe QDMs in the three solvent composition under ambient (Top) and 365 nm (Bottom) light. Samples A-C correspond to Dioxane/Toluene, DMF/Toluene and THF/Toluene 50/50 (v/v) mixtures respectively. Figure S2 (Supporting Information) shows that samples B and C produce significant precipitate at the bottom of the vials after overnight settling.

In the case of the sample prepared in 1,4-dioxane, the obtained CdSe QDMs are clearly visible by TEM (Figure 3 A). Due to electron densities, only the CdSe QDs in the micelle cores are observed. From the TEM images, and by measuring *ca.* 170 QDs, we determined a size distribution corresponding to a mean QD diameter of 3 nm with a population standard deviation of 1 nm. The CdSe QDMs dispersed in a 50/50 mixture of dioxane and toluene (v/v) measured by DLS following filtration through 0.45 μm Teflon filters, have a number-averaged effective hydrodynamic diameter of 20 nm

with a population standard deviation of 5 nm (Figure 3 B), which compares to D_h = 14 nm obtained for the cadmium acrylate-core micelles prepared in 1,4-dioxane (Figure S1). The UV-vis. absorption of the QDM prepared in 1,4-dioxane (Figure S4) is typical of CdSe QDs, with both the excitation and photoluminescence spectra featuring bands that do not change with the excitation wavelength, and are characteristic of quantum confinement effects (Figure 4). [51]

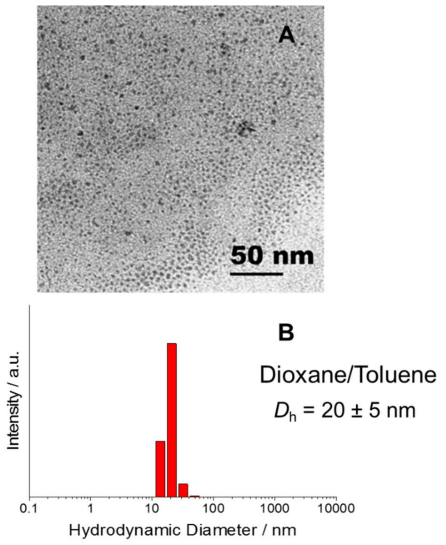

Figure 3. (A) Transmission electron micrograph of CdSe QDMs deposited from dioxane with a mean QD diameter of 3 nm with a population standard deviation of 2 nm, shown with a 50 nm scale bar. (B) Hydrodynamic diameter D_h number distribution generated by CONTIN fit of dynamic light scattering measurements of CdSe QDMs in a 50/50 mixture of dioxane and toluene (v/v), following filtration through 0.45 μm Teflon filters. The average value of D_h was calculated directly from the histogram. The number-averaged effective hydrodynamic diameter is D_h = 20 nm, with a population standard deviation of 5 nm.

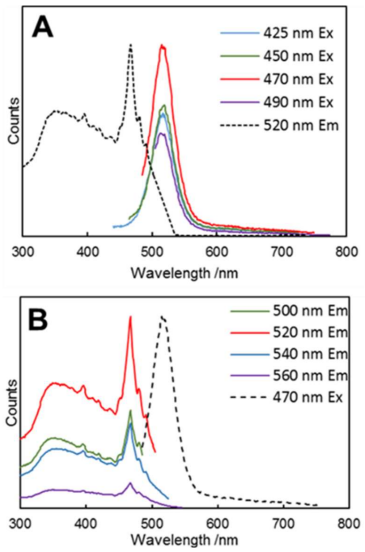

Figure 4. Photoluminescence spectra of CdSe QDMs in a 50/50 mixture of dioxane and toluene (v/v). (A) Emission spectra at four different excitation wavelengths (collected with a 10x neutral density filter, normalized by their relative intensity to the most emissive run, i.e. 470 nm), taken around the exciton peak. Excitation spectrum collected at 520 nm (normalized at λ_{max} = 470 nm) included for reference. (B) Excitation spectra at four different emission wavelengths (normalized by their relative intensity to the most emissive run, i.e. 520 nm). Emission spectrum with excitation at 470 nm (normalized at λ_{max} = 520 nm) included for reference.

The formation of small aggregates in DMF upon addition of cadmium acetate, instead of the homogenous micellar aggregates observed in THF and dioxane, appears to lead to core fusion/aggregation when the CdSe nanocrystals grow in this solvent, leading to the formation of large, colloidally unstable and non-emissive CdSe crystals that precipitate overnight. In the case of THF, although cadmium acetate micelles are initially formed as in dioxane, the micelles are less stable than in dioxane and lead to CdSe nanocrystals with very low emission that precipitate overnight.

Static light scattering of the final CdSe QDMs obtained in dioxane (Figure S2 B) yielded a micelle molecular weight of $M_w = (1.2 \pm 0.4) \times 10^6$ g mol^{-1}. Using the molar mass of the copolymer chain (Table 1), we calculate a micellar aggregation number of 80 ± 27.

Considering the copolymer structure and the colloidal stability of the micelles, these probably have a flower-like structure, with the TTC groups at the apex of each PS "petal", consisting of the central PS block that folds during self-assembly to allow the outermost PAA blocks in each chain to be incorporated into the core, as represented in the cartoon in Scheme 4.

A deeper understanding of the self-assembly behavior of the RAFT copolymer in various solvents is germane to its application as a template for CdSe QDs and gold nanoparticle-QD composite nanostructures. Therefore, in order to gain insight into why stable and emissive CdSe dispersions were obtained in 1,4-dioxane, but not in THF or DMF, we conducted a thorough characterization of the PAA-*b*-PS-TTC-PS-*b*-PAA block copolymer in the different solvents. To probe the different interactions at play, we used a combination of size exclusion chromatography with multi-angle laser light scattering detection (SEC-MALS) and Molecular Dynamics (MD) simulations.

Characterization of the PAA-*b*-PS-TTC-PS-*b*-PAA Block Copolymer. Size exclusion chromatography (SEC) coupled to a mass-sensitive detector, such as viscosity or light scattering, is the most common experimental technique to verify the level of control over copolymer architecture and molecular weight. The combination of a refractive index (RI) detector (sensitive to concentration) with a multi-angle laser light scattering (MALS) detector is particularly advantageous since it offers the possibility of obtaining both absolute molecular weights and chain dimensions along the chromatogram, as well as information of the solvent-polymer interactions.[52] In the case of block copolymers, the characterization by SEC-MALS is complicated by differences in solvent quality for the blocks, which can lead to the formation of micellar aggregates in the eluting solvent. Although the self-assembly

behavior is critical to the application of the copolymers as templates for nanostructured materials, it provides a serious challenge to the definitive SEC-MALS characterization of their molecular weights, since aggregation in the eluting solvent can lead to erroneous assignment of molecular weights and strong deviations in measured molecular weights and chain dimensions in different solvents. This is aggravated for copolymers carrying charged monomers since salts are sometimes added to the solvent in order to screen electrostatic interactions,[53] potentially leading to further changes in aggregation behavior.

The SEC-MALS characterization of asymmetric poly(styrene-*b*-acrylic acid) copolymers is described in the literature, but often yields different values of apparent molecular weight and size dispersity in tetrahydrofuran (THF), [54] *N,N*-dimethylformamide (DMF) [55] and 1,4-dioxane (dioxane).[35][35] These discrepancies are probably related to the different results we obtained in the self-assembly of our block copolymer and subsequent preparation of the QDMs. In order to clarify this relation, we measured the molecular weight and dimensions of our copolymers by SEC-MALS in the three solvents, 1,4-dioxane, THF and DMF, varying the dielectric properties of the last two by adding lithium salts. Both THF and dioxane are good solvents for polystyrene (PS), while DMF is a marginally good solvent for PS (Mark-Houwink-Sakurada exponents of 0.749, [56] 0.694 [57] and 0.603,[58] respectively). No data on the quality of either THF or DMF to PAA could be found in the literature, while dioxane has been reported to be a θ solvent for PAA at 30 °C (the working temperature of the SEC-MALS in these experiments). [59]

The chromatograms obtained in THF (Figure 5 A) show that the peaks are broader and displaced towards lower elution volumes (*i.e.* higher hydrodynamic volumes) compared to those obtained when we used THF with 0.2 M LiCl (Figure 5 B) or with 0.15 M LiBr (Figure S5). The same trend was observed when using DMF as eluent and we added 0.15 M LiBr (Figure S5). This behavior suggests the presence of electrostatically-mediated aggregation of copolymer chains that change with

Formatted: Endnote Reference

the addition of salt, which is supported by the shift between MALS and RI signals in Figure 5. These are large polymer aggregates with a broad size distribution, as indicated by the radius of gyration curve obtained from the light scattering (SEC-MALS) experiments (Figure 5 and Figure S5). The aggregates are formed by the collapse of the polymer chains in poor solvents (THF and DMF) to form globules that aggregate into unstable colloidal structures. On the other hand, if we use dioxane, the MALS and RI curves are similar, with maxima appearing at the same elution volume (Figure 6), as expected for non-aggregated (isolated) chains with low size dispersity.

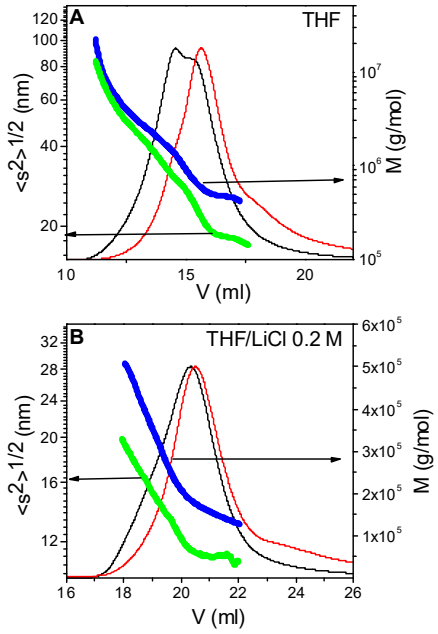

Figure 5. Refractive index signal (*red*) and the MALS signal at 90º (*black*) versus elution volume. Molecular weight (*blue*) and radius of gyration (*green*) calculated for each elution volume for the copolymer in THF (A) and THF with 0.2 M LiCl (B).

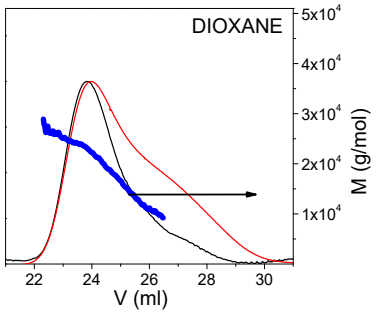

Figure 6. Refractive index signal (*red*) and the MALS signal at 90º (*black*) versus elution volume. Molecular weight (*blue*) calculated for each elution volume for the copolymer in dioxane.

In order to understand the effect of the acrylic acid (AA) units in the aggregation of the block copolymer in THF and DMF, the PAA-*b*-PS-TTC-PS-*b*-PAA copolymer was silylated by converting the AA of the PAA blocks using (trimethylsilyl)-diazomethane.[43] When the modified polymer was analyzed in THF (Figure 7) we observed that the chromatograms are similar to those obtained for the non-modified copolymer in dioxane, with the maxima of the MALS and RI curves appearing at the same elution volume. This shows that the polar nature of the PAA groups are germane to the aggregation behavior of the copolymer in THF, and further suggests that dioxane is a nonselective solvent for the copolymer, since silylation is not required to suppress aggregation in that solvent.

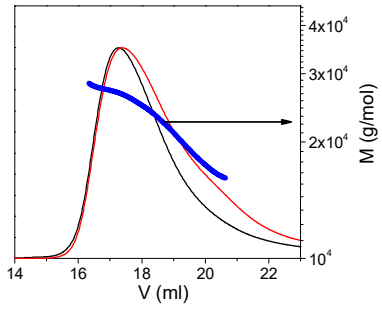

Figure 7. Refractive index signal (*red*) and the MALS signal at 90º (*black*) versus elution volume. Molecular weight (*blue*) calculated for each elution volume for the silylated copolymer in THF.

The molecular weight and radius of gyration *versus* elution volume obtained for the copolymer in THF (Figure 5 A) and DMF (Figure S5 A) indicate poor chromatographic separation since they do not cover the full range of the MALS and refraction index peaks. The addition of salt displaces the curves to lower values of molecular weight and radius of gyration, due to the disruption of the aggregates: in THF, the lowest values of molecular weight are obtained with 0.2 M LiCl (Figure 5 B); in DMF, the addition of 0.15 M LiBr (Figure S5 B) produces a significantly larger effect on the decrease of molecular weight and radius of gyration than the addition of the same salt to THF. Table 1 summarizes the average values of the molecular weight and the radius of gyration of the copolymer and its size dispersity in different solvents.

Although polymer aggregates can be partially disrupted by salt addition in THF and DMF, even for the more effective salts (0.2 M LiCl in THF and 0.15 M LiBr in DMF), the determined molecular weights are considerably larger than the value determined in dioxane (Figure 6, $M_w = 1.6 \times 10^4$ g mol^{-1}; $M_w/M_n = 1.13$), which is very close to the values obtained for the methylated polymer in THF after correction for the additional methyl groups (Figure 7, $M_w = 1.5 \times 10^4$ g mol^{-1}; $M_w/M_n = 1.10$). The later values are also in good agreement with the molecular weight estimated from the conversion obtained

by ^{1}H NMR (1.5×10^{4} g mol^{-1}). For the copolymer in dioxane, the size dispersity measured by SEC-MALS is typical of RAFT polymerization.

Table 1. Average molecular weight (M_w), dispersity (M_w/M_n) and root mean square radii of gyration $\langle s_z^2 \rangle^{1/2}$ calculated by SEC-MALS for the PAA-*b*-PS-TTC-PS-*b*-PAA copolymer in different solvents.

Solvent	M_w/ 10^5 (g/mol)	$\langle s_z^2 \rangle^{1/2}$ (nm)	M_w /M_n
THF	7.6	22	1.5
THF/0.15 M LiBr	6.1	22	1.6
THF/0.20 M LiCl	1.9	12	1.3
DMF	2.7	75	1.7
DMF/0.15M LiBr	0.34	13	1.2
Dioxane[b]	**0.16**	**5.3** [a]	**1.1**
Silylated copolymer in THF	0.23	-	1.1

[a] Estimated from the hydrodynamic radius measured by DLS (see text).

[b] Values in this solvent correspond to single copolymer chains whereas values in other solvents represent various states of copolymer chain aggregation (see discussion in text).

It is not possible to determine the radius of gyration curve for the non-aggregated copolymer in dioxane, nor the methylated copolymer in THF, because its small value is beyond the detection limit of MALS detector. However, this value can be estimated using dynamic light scattering (DLS) measurements. The hydrodynamic radius of the copolymer chains at low concentration in dioxane, determined by DLS, is $R_h = (3 \pm 1)$ nm. Burchard has shown that for random coils in good solvents, the ratio R_g / R_h can be estimated to be 1.78. [60] Thus the measured value of R_h corresponds to a radius of gyration of $R_g = R_h \times 1.78 = 5.3$ nm, which is significantly smaller than the R_g measured by SEC-

MALS for the copolymer aggregates in both THF and DMF (Table 1). The hydrodynamic radius of the copolymer in dioxane is practically constant up to polymer concentrations of ca. 1.5 g/L (Figure S6 A), with higher concentrations showing aggregate formation (Figure S7) that prevents the determination of the radius of gyration and second virial coefficient by static light scattering (SLS, Figure S6 B). We thus conclude that, in order to have free copolymer chains in solution, characterization of this and similar copolymers by SEC-MALS, DLS, and SLS should be carried out below 1.5 g/L in dioxane.

Finally, to evaluate the relative size of the two PS-*b*-PAA sections on either side of the central TTC group, the TTC group was cleaved with hexylamine. The molecular weight of the resulting PS-PAA chains was half the initial value, indicating that the tetra-block copolymer has a symmetrical architecture, as expected from the structure of the trithiocarbonate chain transfer agent.

Molecular Dynamics (MD) Simulations. To better understand the interactions between the different blocks in the copolymer and the various solvents used in block copolymer characterization and self-assembly experiments, we performed molecular dynamics (MD) simulations in four model tetrablock oligomers containing blocks of 10 repeat units each (Scheme 3): two type S oligomers composed of a central trithiocarbonate (TTC) unit flanked by two inner styrene blocks and two outer blocks of either acrylic acid (SA) or methyl acrylate ester (SE); and two type C oligomers without a central TTC unit and two outer blocks of either acrylic acid (CA) or methyl acrylate ester (CE).

The simulations allow the calculation of distances between different atoms in the oligomers, and between various atoms in the oligomers and the solvent molecules. We have selected the following three types of atoms to follow within each oligomer chain, marked with an asterisk in Scheme 3:

1.) the central sulfur atom of the TTC group of type S oligomers (one atom per oligomer, labeled S*);

2) the oxygen atom of the carboxyl groups of type S and type C oligomers (22 atoms per oligomer chain, labeled O*); and

3) the aromatic C atom of each phenyl group that is linked to the chain of the type S (20 atoms per oligomer chain, labeled C*) and type C oligomers (22 atoms per oligomer chain, labeled C*).

The oligomer-solvent distances correspond to the average separation relative to the center of mass of each of the 2,000 solvent molecules in each system. Distances of interest were computed for all the configurations recorded during the MD trajectories. The radial correlation function $g(r)$ was calculated from the ratio between the probability of finding two atoms at a distance $r \pm \delta r$ to the same probability for a random distribution of atoms, using $\delta r = 0.01$ nm.

MD Simulations of Type S Methyl Acrylate Oligomers in THF (SE-THF). The simulation results obtained for the methylated oligomer with a central TTC group in THF (SE-THF) were used as reference to which the other systems were compared. Figure S8 shows the radial correlation function $g(r)$ for the intramolecular (Figure S8 A), intermolecular (Figure S8 B) and oligomer-solvent distances (Figure S8 C). The broad, approximately Gaussian, profile in Figure S8 A shows that the oligomer chain is in a coiled conformation, without observable correlation among different parts of the chain. THF is a good solvent for PS and consequently the central part of the oligomer is quite extended producing a rather large separation (at least by 2.5 nm) among the O* atoms of the acrylic units at both ends of the oligomer, without noticeable correlation. On the other hand, Figure S8 B shows a noticeable displacement of the intermolecular O*…O* peaks of the correlation function towards shorter distances, but the value of $g(r)$ is close to 1 from 1 to 4 nm, which indicates absence of correlation (and interaction) between the methylated groups in different chains. Moreover, the S*…S* interchain correlation shows a sharp peak at ca. 0.5 nm which is attributed to the hydrophobicity of the trithiocarbonate group contributing to the approximation of different oligomers in a polar solvent such as THF.

The oligomer-solvent correlation curves shown in Figure S8 C indicate that the coiled chains are uniformly solvated, with no evidence of preferential solvation of any part of the methylated chains

in THF. The distribution of solvent molecules is similar around the S* atoms (central part of the oligomer chains), the C* atoms and the O* atoms (chain ends). The first solvation shell is placed at a slightly larger distance in the case of C* atoms, but this is due to the larger size of the phenyl groups to which the C* atoms belong.

MD Simulations of Type S Acrylic Acid Oligomers in THF (SA-THF). Figure S9 shows that the distribution function of intramolecular distances for both S*…O* and O*…O* are similar in SE-THF and SA-THF (Figures S8 and S9). This is a consequence of THF being a good solvent for PS, which favors the extended conformations of the central part of the chain, keeping the acrylic acids units away from each other. On the other hand, the correlation of S*…S* intermolecular distances observed at $r \approx 0.5$ nm for SE-THF (Figure S8 B) is not present in SA-THF (Figure S9 B). Instead, a much stronger correlation of the O* … O* intermolecular distances is observed at approximately the same value of r. The intensity and sharpness of this peak suggest that several oligomers could aggregate through the acrylic units. Figure S9 C shows that the correlation of the solvent molecules with the S*, C* and O* atoms is similar to SE-THF (Figure S8 C), indicating that the chains are uniformly solvated. The same result is observed for the systems SA-THF/Li (Figure S10 C) and SA-Dioxane (Figure S11 C).

MD Simulations of Type S Acrylic Acid Oligomers in THF with LiCl Salt (SA-THF/Li). Figure S10 shows that the addition of salt to THF does not change the intramolecular O*…O* and S*…O* distance correlations, and that the correlation for the intermolecular S*…S* distance is also very similar to that of SA-THF shown above. However, addition of the salt modifies the intermolecular interactions among acrylic groups which fall in between those of SE-THF and SA-THF (compare the broken lines in Figures S5 B, S6 B and S7 B). These results indicate that, although aggregation persists, salt addition helps disrupt the interactions among the acrylic acid units of different chains.

MD Simulations of Type S Acrylic Acid Oligomers in Dioxane (SA-Dioxane). Figure S11 shows that the correlations for intramolecular S*…S* and O*…O* distances are very similar to those obtained for both SA and SE in THF, although the peaks are shifted towards lower values of *r* due to the fact that dioxane is a worse solvent for PS than THF. Although the S*…S* intermolecular distance distribution is shifted to higher values, indicating a lower tendency to aggregation driven by the trithiocarbonate group, the O*…O* intermolecular distances are similar to those in THF. This result suggests that, at least for the simulated oligomers, the tendency for aggregation (experimentally observed in THF, but not in dioxane), is mainly driven by the TTC groups rather than by the PAA blocks.

MD Simulations of Oligomers without the TTC Group. Finally, in order to understand the role of the central trithiocarbonate (TTC) group we considered oligomers without this group. The CE and CA oligomers used in these calculations are formed by a block of 22 repeat units of styrene flanked on each side by a block of 11 repeat units of either acrylic acid (CA oligomer) or methyl acrylic ester (CE oligomer) as shown in Scheme 3. The carbon atom of the central CH_2 group of both CE and CA oligomers is used as the origin to measure the distances for the evaluation of the correlation functions (similarly to the central S atom of the SE and SA oligomers), and is represented as CC in Figure S12. The most important conclusion of the calculations is that when the TTC group is not present (CE-THF; solid line in Figure S12 B), the sharp peak appearing at *ca.* 0.4 - 0.5 in the SE-THF case (Figure S8 B) disappears, suggesting that the TTC hydrophobic interactions play an important role in the aggregation of TTC-containing chains in THF.

Comparing the results computed for CA-THF (Figure S12) with those of SA-THF (Figure S9), the O*…O* distances (both intra and inter) are very similar for both systems, the distribution for intermolecular CC…CC distance (solid line in Figure S12 B) is also similar to the S*…S* intermolecular distance distribution in SA-THF (solid line in Figure S9 B). The main difference is that

for S*...S* we observe values of $g(r) > 1$ for very short distances ($r < 1$ nm), whereas the CC…CC intermolecular distance distribution is shifted to higher values of r. This displacement indicates a lower tendency to aggregation in the absence of the TTC group. Thus we conclude that the TTC group is responsible, together with the acrylic groups, for the strong aggregations among the oligomers in THF solutions.

Discussion of SEC-MALS and MD Results and Importance for Characterization and Self-Assembly of PAA-*b*-PS-TTC-PS-*b*-PAA. The TTC group located precisely at the center of our unique copolymers gives us a chemical handle on binding gold nanostructures at a controlled distance from the CdSe QDs prepared by using the self-assembled copolymer template. However, the TTC group also presents special challenges, not only for copolymer characterization, but also for selecting appropriate conditions for its self-assembly. This adds to the problems already reported in the literature for characterizing PS-b-PAA chains without the TTC. Our detailed SEC-MALS and MD results helped us identified the main causes for the uncontrolled aggregation of the copolymer in various solvents, pointing the way to its successful characterization and controlled self-assembly conditions. While MD calculations suggest that the TTC groups play a pivotal role in the aggregation of the simulated oligomers, absent only when dioxane is used as solvent, the interaction between PAA blocks is expected to become more important for larger chains. In fact, this interaction was proved a key factor in the SEC-MALS experiments, in which aggregation could be eliminated by reducing the interaction between PAA blocks, both in THF by methylation of the copolymer, and by dissolving the copolymer in dioxane. These results allowed us to understand the appropriate conditions for the characterization of the block copolymer chains, and to select the best strategy to achieve their controlled self-assembly for application as nanoparticle scaffolds.

The fact that we could only measure isolated PAA-*b*-PS-TTC-PS-*b*-PAA copolymer chains in dioxane, explains why only in this solvent it was possible to obtain the desired templates to prepare CdSe QDs by adding cadmium acetate to selectively associate the PAA blocks. The lower stability of cadmium acetate micelles prepared in THF and the heterogeneous aggregation in DMF ultimately resulted in extensive aggregation and precipitation of non-emissive CdSe crystals.

Conclusions

We used RAFT to prepare a symmetric tetrablock copolymer of precisely controlled architecture composed of a trithiocarbonate (TTC) central group, two polystyrene inner blocks, and two acrylic acid outer blocks. The TTC functional group offers the capability of using this copolymer as a unique scaffold for quantum dot-gold nanoparticle composites, but also introduces challenges to controlled self-assembly, due to its contributions to the aggregation behavior of the chains in various solvents. This was evidenced by our unsuccessful attempts to produce well-dispersed and luminescent CdSe QDs in RAFT copolymer templates using DMF and THF as dispersing solvents.

We carried out a thorough SEC-MALS study of the copolymer in different solvents to better understand its aggregation behavior. In THF and DMF, the copolymer has a strong tendency to aggregate, as evidenced by the measured high molecular weights, with addition of salts lowering molecular weights but not to the level of single chains. In dioxane, the results agreed with those obtained for the modified copolymer in THF after methylation of acrylic acid groups to suppress aggregation, suggesting that dioxane is a nonselective solvent for the copolymer, capable of dispersing single chains. Further, MD simulations showed that hydrogen bonding between the acrylic acid units is the probable main cause of interchain interactions leading to aggregation in THF and DMF, but not in dioxane. MD simulations also confirmed that salt addition to THF and DMF only partially disrupt ion

pairs formed by incomplete dissociation of the acid units, and that the hydrophobic central TTC group contributes to the stabilization of the aggregates in THF and DMF.

Controlled self-assembly *en route* to nanostructure synthesis was achieved by using dioxane to fully dissolve the copolymer and then adding cadmium acetate to induced segregation of the PAA blocks that self-assemble into spherical inverted micelles of homogeneous size. These micelles were then used as nanoreactors in the templated synthesis of a single CdSe quantum dot within each core, expanding our earlier demonstration of CdS synthesis in the same copolymer to a more common and useful color-tunable emitter. This combination of controlled RAFT polymerization, SEC-MALS measurement and MD modeling in a variety of solvents, and the demonstrated versatility of nanoparticle templating, provides the framework for a general and powerful strategy for surface plasmon-enhanced PL emission in nanoparticle-based devices.

Supporting Information

Additional SEC-MALS experimental results for the characterization of the PAA-*b*-PS-TTC-PS-*b*-PAA copolymer (and its aggregates) in different solvents, average hydrodynamic diameter calculated from the number-weighted distribution obtained by dynamic light scattering of the copolymer in 1,4-dioxane, SLS Zimm plots of the coplymer and the QDMs in 1,4-dioxane, and plots of the radial correlation functions obtained from the MD trajectories for the simulated oligomers in different solvents. This material is available free of charge via the Internet at http://pubs.acs.org

Acknowledgements

This work was partially supported by Fundação para a Ciência e a Tecnologia (FCT-Portugal) and COMPETE (FEDER), within projects UID/NAN/50024/2013 and PTDC/CTM-POL/3698/2014. T.R. also thank FCT for Post-Doc grant SFRH/BPD/96707/2013.

References

(1) Whitesides, G. M.; Grzybowski, B. Self-Assembly at All Scales. *Science* **2002,** *295*, 2418-2421.

(2) Cummins, C. C.; Schrock, R. R.; Cohen, R. E. Synthesis of zinc sulfide and cadmium sulfide within ROMP block copolymer microdomains. *Chem. Mater.* **1992,** *4*, 27-30.

(3) Möller, M.; Spatz, J. P.; Roescher, A. Gold nanoparticles in micellar poly(styrene)-b-poly(ethylene oxide) films—size and interparticle distance control in monoparticulate films. *Adv. Mater.* **1996,** *8*, 337-340.

(4) Moffitt, M.; Eisenberg, A. Size Control of Nanoparticles in Semiconductor-Polymer Composites. 1. Control via Multiplet Aggregation Numbers in Styrene-Based Random Ionomers. *Chem. Mat.* **1995,** *7*, 1178-1184.

(5) Wang, C. W.; Moffitt, M. G. Use of Block Copolymer-Stabilized Cadmium Sulfide Quantum Dots as Novel Tracers for Laser Scanning Confocal Fluorescence Imaging of Blend Morphology in Polystyrene/Poly(methyl methacrylate) Films. *Langmuir* **2005,** *21*, 2465-2473.

(6) Shang, L.; Dong, S.; Nienhaus, G. U. Ultra-small fluorescent metal nanoclusters: Synthesis and biological applications. *Nano Today* **2011,** *6*, 401-418.

(7) Mai, Y.; Eisenberg, A. Self-assembly of block copolymers. *Chem. Soc. Rev.* **2012,** *41*, 5969-5985.

(8) Lee, J.; Govorov, A. O.; Kotov, N. A. Nanoparticle Assemblies with Molecular Springs: A Nanoscale Thermometer. *Angew. Chem.* **2005,** *117*, 7605-7608.

(9) Wang, M.; Kumar, S.; Lee, A.; Felorzabihi, N.; Shen, L.; Zhao, F.; Froimowicz, P.; Scholes, G. D.; Winnik, M. A. Nanoscale Co-organization of Quantum Dots and Conjugated Polymers Using Polymeric Micelles As Templates. *J. Am. Chem. Soc.* **2008,** *130*, 9481-9491.

(10) Nie, Z.; Petukhova, A.; Kumacheva, E. Properties and emerging applications of self-assembled structures made from inorganic nanoparticles. *Nat Nano* **2010,** *5*, 15-25.

(11) Moffitt, M. G. Self-Assembly of Polymer Brush-Functionalized Inorganic Nanoparticles: From Hairy Balls to Smart Molecular Mimics. *The Journal of Physical Chemistry Letters* **2013,** *4*, 3654-3666.

(12) Ribeiro, T.; Prazeres, T. J. V.; Moffitt, M.; Farinha, J. P. S. Enhanced Photoluminescence from Micellar Assemblies of Cadmium Sulfide Quantum Dots and Gold Nanoparticles. *J. Phys. Chem. C* **2013,** *117*, 3122-3133.

(13) Ray, K.; Badugu, R.; Lakowicz, J. R. Metal-Enhanced Fluorescence from CdTe Nanocrystals: A Single-Molecule Fluorescence Study. *J. Am. Chem. Soc.* **2006,** *128*, 8998-8999.

(14) Liu, N.; Prall, B. S.; Klimov, V. I. Hybrid Gold/Silica/Nanocrystal-Quantum-Dot Superstructures: Synthesis and Analysis of Semiconductor−Metal Interactions. *J. Am. Chem. Soc.* **2006,** *128*, 15362-15363.

(15) Fedutik, Y.; Temnov, V.; Woggon, U.; Ustinovich, E.; Artemyev, M. Exciton−Plasmon Interaction in a Composite Metal−Insulator−Semiconductor Nanowire System. *J. Am. Chem. Soc.* **2007,** *129*, 14939-14945.

(16) Kim, B.-S.; Taton, T. A. Multicomponent Nanoparticles via Self-Assembly with Cross-Linked Block Copolymer Surfactants. *Langmuir* **2007,** *23*, 2198-2202.

(17) Chen, C. W.; Wang, C. H.; Wei, C. M.; Chen, Y. F. Tunable emission based on the composite of Au nanoparticles and CdSe quantum dots deposited on elastomeric film. *Applied Physics Letters* **2009,** *94*, 071906.

(18) Quach, A. D.; Crivat, G.; Tarr, M. A.; Rosenzweig, Z. Gold Nanoparticle−Quantum Dot−Polystyrene Microspheres as Fluorescence Resonance Energy Transfer Probes for Bioassays. *J.*

Am. Chem. Soc. **2011,** *133*, 2028-2030.

(19) Jung, D.-R.; Kim, J.; Nam, S.; Nahm, C.; Choi, H.; Kim, J. I.; Lee, J.; Kim, C.; Park, B. Photoluminescence enhancement in CdS nanoparticles by surface-plasmon resonance. *Applied Physics Letters* **2011,** *99*, 041906.

(20) Zeng, Q.; Zhang, Y.; Liu, X.; Tu, L.; Kong, X.; Zhang, H. Multiple homogeneous immunoassays based on a quantum dots-gold nanorods FRET nanoplatform. *Chem. Comm.* **2012,** *48*, 1781-1783.

(21) Zhang, J.; Ma, N.; Tang, F.; Cui, Q.; He, F.; Li, L. pH- and Glucose-Responsive Core–Shell Hybrid Nanoparticles with Controllable Metal-Enhanced Fluorescence Effects. *ACS Applied Materials & Interfaces* **2012**, *4*, 1747-1751.

(22) Tang, F.; Ma, N.; Tong, L.; He, F.; Li, L. Control of Metal-Enhanced Fluorescence with pH- and Thermoresponsive Hybrid Microgels. *Langmuir* **2012,** *28*, 883-888.

(23) Cui, Q.; He, F.; Li, L.; Möhwald, H. Controllable metal-enhanced fluorescence in organized films and colloidal system. *Adv. Colloid Interface Sci.* **2014,** *207*, 164-177.

(24) Braunecker, W. A.; Matyjaszewski, K. Controlled/living radical polymerization: Features, developments, and perspectives. *Progress in Polymer Science* **2007,** *32*, 93-146.

(25) Moad, G.; Rizzardo, E.; Thang, S. H. Toward Living Radical Polymerization. *Accounts of Chemical Research* **2008,** *41*, 1133-1142.

(26) Hawker, C. J.; Bosman, A. W.; Harth, E. New Polymer Synthesis by Nitroxide Mediated Living Radical Polymerizations. *Chem. Rev.* **2001,** *101*, 3661-3688.

(27) Matyjaszewski, K.; Xia, J. Atom Transfer Radical Polymerization. *Chem. Rev.* **2001,** *101*, 2921-2990.

(28) Matyjaszewski, K.; Tsarevsky, N. V. Nanostructured functional materials prepared by atom transfer radical polymerization. *Nat Chem* **2009,** *1*, 276-288.

(29) Moad, G.; Rizzardo, E.; Thang, S. H. Living Radical Polymerization by the RAFT Process – A Third Update. *Australian Journal of Chemistry* **2012,** *65*, 985-1076.

(30) Perrier, S.; Takolpuckdee, P. Macromolecular design via reversible addition–fragmentation chain transfer (RAFT)/xanthates (MADIX) polymerization. *Journal of Polymer Science Part A: Polymer Chemistry* **2005,** *43*, 5347-5393.

(31) Favier, A.; Charreyre, M.-T. Experimental Requirements for an Efficient Control of Free-Radical Polymerizations via the Reversible Addition-Fragmentation Chain Transfer (RAFT) Process. *Macromolecular Rapid Communications* **2006,** *27*, 653-692.

(32) Moad, G.; Rizzardo, E.; Thang, S. H. Radical addition–fragmentation chemistry in polymer synthesis. *Polymer* **2008,** *49*, 1079-1131.

(33) Riess, G. Micellization of block copolymers. *Progress in Polymer Science* **2003,** *28*, 1107-1170.

(34) Zhang, L.; Eisenberg, A. Multiple Morphologies of "Crew-Cut" Aggregates of Polystyrene-b-poly(acrylic acid) Block Copolymers. *Science* **1995,** *268*, 1728-1731.

(35) Choucair, A.; Lim Soo, P.; Eisenberg, A. Active Loading and Tunable Release of Doxorubicin from Block Copolymer Vesicles. *Langmuir* **2005,** *21*, 9308-9313.

(36) Wu, J.; Eisenberg, A. Proton Diffusion across Membranes of Vesicles of Poly(styrene-b-acrylic Acid) Diblock Copolymers. *J. Am. Chem. Soc.* **2006,** *128*, 2880-2884.

(37) Wang, X.; Luo, Y.; Li, B.; Zhu, S. Ab Initio Batch Emulsion RAFT Polymerization of Styrene Mediated by Poly(acrylic acid-b-styrene) Trithiocarbonate. *Macromolecules* **2009,** *42*, 6414-6421.

(38) He, W.-D.; Sun, X.-L.; Wan, W.-M.; Pan, C.-Y. Multiple Morphologies of PAA-b-PSt Assemblies throughout RAFT Dispersion Polymerization of Styrene with PAA Macro-CTA. *Macromolecules* **2011,** *44*, 3358-3365.

(39) Henglein, A. Small-particle research: physicochemical properties of extremely small colloidal metal and semiconductor particles. *Chem. Rev.* **1989,** *89*, 1861-1873.

(40) Kim, S.; Bawendi, M. G. Oligomeric Ligands for Luminescent and Stable Nanocrystal Quantum Dots. *J. Am. Chem. Soc.* **2003,** *125*, 14652-14653.

(41) Resch-Genger, U.; Grabolle, M.; Cavaliere-Jaricot, S.; Nitschke, R.; Nann, T. Quantum dots versus organic dyes as fluorescent labels. *Nat Meth* **2008,** *5*, 763-775.

(42) Lai, J. T.; Filla, D.; Shea, R. Functional Polymers from Novel Carboxyl-Terminated Trithiocarbonates as Highly Efficient RAFT Agents. *Macromolecules* **2002,** *35*, 6754-6756.

(43) Lessard, B.; Marić, M. Effect of an Acid Protecting Group on the "Livingness" of Poly(acrylic acid-ran-styrene) Random Copolymer Macroinitiators for Nitroxide-Mediated Polymerization of Styrene. *Macromolecules* **2008,** *41*, 7881-7891.

(44) Jackson, C.; Chen, Y.-J.; Mays, J. W. Size exclusion chromatography with multiple detectors: Solution properties of linear chains of varying flexibility in tetrahydrofuran. *Journal of Applied Polymer Science* **1996,** *61*, 865-874.

(45) Dietrich, V. W.; Basch, A. Nachweis von mikrogelen in polyamiden durch lichtstreuung. *Die Angewandte Makromolekulare Chemie* **1974,** *40*, 159-172.

(46) Huglin, M. B.; O'Donohue, S. J.; Radwan, M. A. Refractometric and light scattering parameters at 633 nm for polystyrene solutions. *European Polymer Journal* **1989,** *25*, 543-547.

(47) Marcelo, G.; J. V. Prazeres, T.; Charreyre, M.-T.; Martinho, J. M. G.; Farinha, J. P. S. Thermoresponsive Micelles of Phenanthrene-α-end-labeled Poly(N-decylacrylamide-b-N,N-diethylacrylamide) in Water. *Macromolecules* **2010,** *43*, 501-510.

(48) http://www.amber.ucsf.edu/amber/amber.html; http://www.amber.ucsf.edu/amber/dbase.html;

http://pharmacy.man.ac.uk/amber/

(49) MOPAC, Quantum Chemistry Program Exchange (Department of Chemistry, Indiana University, Bloomington, IN).

(50) Allen, M. P.; Tildesley, D. J. *Computer Simulation of Liquids*, Clarendon: Oxford, **1987**.

(51) Wang, C. W.; Moffitt, M. G. Surface-Tunable Photoluminescence from Block Copolymer-Stabilized Cadmium Sulfide Quantum Dots. *Langmuir* **2004,** *20*, 11784-11796.

(52) Marcelo, G.; Tarazona, M. P.; Saiz, E. Solution properties of poly(diallyldimethylammonium chloride) (PDDA). *Polymer* **2005,** *46*, 2584-2594.

(53) Marcelo, G.; Mendicuti, F.; Saiz, E.; Tarazona, M. P. Combination of SEC-MALS and Fluorescence with Molecular Dynamics Simulations for the Analysis of Ionomer Dimensions in Solution. Application to Poly(2-acrylamido-2-methyl-1-propanesulfonic acid-co-styrene). *Macromolecules* **2007,** *40*, 1311-1320.

(54) Burguière, C.; Pascual, S.; Bui, C.; Vairon, J.-P.; Charleux, B.; Davis, K. A.; Matyjaszewski, K.; Bétremieux, I. Block Copolymers of Poly(styrene) and Poly(acrylic acid) of Various Molar Masses, Topologies, and Compositions Prepared via Controlled/Living Radical Polymerization. Application as Stabilizers in Emulsion Polymerization. *Macromolecules* **2001,** *34*, 4439-4450.

(55) Rowe, M. D.; Hammer, B. A. G.; Boyes, S. G. Synthesis of Surface-Initiated Stimuli-Responsive Diblock Copolymer Brushes Utilizing a Combination of ATRP and RAFT Polymerization Techniques. *Macromolecules* **2008,** *41*, 4147-4157.

(56) Spatorico, A. L.; Coulter, B. Molecular weight determinations by gel-permeation chromatography and viscometry. *Journal of Polymer Science: Polymer Physics Edition* **1973,** *11*, 1139-1150.

(57) Wagner, H. L. The Mark–Houwink–Sakurada Equation for the Viscosity of Atactic Polystyrene.

Journal of Physical and Chemical Reference Data **1985,** *14*, 1101-1106.

(58) Tsimpris, C. W.; Suryanarayanan, B.; Mayhan, K. G. Intrinsic viscosity—molecular weight relationship for polystyrene in N,N-dimethylformamide. *Journal of Polymer Science Part A-2: Polymer Physics* **1972,** *10*, 1837-1839.

(59) Mabire, F.; Audebert, R.; Quivoron, C. Flocculation properties of some water-soluble cationic copolymers toward silica suspensions: A semiquantitative interpretation of the role of molecular weight and cationicity through a "patchwork" model. *Journal of Colloid and Interface Science* **1984,** *97*, 120-136.

(60) Burchard, W. *Static and dynamic light scattering approaches to structure determination of biopolymers. In Laser Light Scattering in Biochemistry*. (Harding, S. E.; Sattelle, D. B.; Bloomfield, V. A. editors). Royal Society of Chemistry: Cambridge, **1992**.